Advances in Science and Technology Research Journal

Advances in Science and Technology Research Journal, 2026, 20(5), 171–184
https://doi.org/10.12913/22998624/215814
ISSN 2299-8624, License CC-BY 4.0

Received: 2025.11.17
Accepted: 2026.03.15
Published: 2026.04.01

Thermo-mechanical behavior of Cu/SS316L dissimilar welded joints for heat pipe applications

Azwinur[1,2], Agus Suprihanto[1], Mukhsinun Hadi Kusuma[3*], Khoiri Rozi[1], Usman Usman[2], Surya Dharma[4]

[1] Department of Mechanical Engineering, Faculty of Engineering, Diponegoro University, Tembalang, 50275, Semarang, Central Java, Indonesia
[2] Department of Mechanical Engineering, Politeknik Negeri Lhokseumawe, Lhokseumawe 24301, Aceh, Indonesia
[3] Research Center for Nuclear Reactor Technology, Research Organization for Nuclear Energy, National Research and Innovation Agency, Kawasan Sains Terpadu B.J. Habibie Serpong, Tangerang Selatan, 15314, Indonesia
[4] Department of Mechanical Engineering, Politeknik Negeri Medan, Kota Medan, Sumatera Utara, 20155, Indonesia
* Corresponding author's e-mail: mhad001@brin.go.id

ABSTRACT

Dissimilar welding between copper (Cu) and stainless steel 316L (SS316L) is essential for heat pipe applications that require high thermal conductivity combined with adequate mechanical integrity. However, the large mismatch in thermal and metallurgical properties between Cu and SS316L complicates joint optimization. This study investigates the effect of heat input (HI) during TIG welding with an ERCuSi-A filler on the microstructure, mechanical behavior, and thermal conductivity of Cu/SS316L dissimilar joints. Three heat input levels (1.41, 2.02, and 2.04 kJ/mm) were applied under identical welding conditions. Microstructural evaluation was performed using optical microscopy and Scanning Electron Microscopy coupled with energy-dispersive x-ray spectroscopy (SEM–EDS) to assess grain evolution, elemental diffusion, and weld metal homogeneity. Tensile testing showed that fractures consistently occurred in the Cu heat-affected zone, indicating that the Cu-rich weld metal was mechanically stronger than the copper base material. Increasing heat input promoted grain coarsening, SS-rich particle agglomeration, and microstructural heterogeneity. Thermal conductivity decreased after welding, with measured values of approximately 264, 198, and 111 W/m·K for heat inputs of 1.41, 2.02, and 2.04 kJ/mm, respectively, lying between those of Cu and SS316L. Overall, a low heat input of 1.41 kJ/mm provided the most favorable balance between mechanical integrity, microstructural stability, and thermal conductivity. These findings highlight the importance of precise heat input control when designing Cu/SS316L welded joints for heat pipe systems.

Keywords: dissimilar metal welding, Cu/SS316L, TIG, thermal conductivity, heat pipe.

INTRODUCTION

Heat pipes become a potential passive system technology to be used for various applications due to their high thermal performance and ability as a heat exchanger, including nuclear installations [1–2]. These devices utilize the latent heat of vaporization to transport heat with minimal temperature differences [3]. Heat pipes have shown significant potential in nuclear technologies, such as space power systems, microreactors, and spent fuel pool cooling [4–5]. Kusuma et al. [6] investigated a passive cooling system for spent nuclear fuel pools using a vertical wickless heat pipe. Their experimental and simulation results demonstrated excellent thermal performance, achieving a thermal resistance as low as 0.016 ± 0.0006 °C/W under optimal conditions,

including low initial pressure and an 80% evaporator filling ratio. This study highlights the potential of wickless heat pipes as an effective passive cooling strategy in nuclear safety applications [6]. Beyond nuclear systems, heat pipes have also been widely applied in other thermal management fields such as electronic cooling, HVAC systems, solar energy, and waste heat recovery [3]. In the context of microreactors, they offer passive heat removal solutions alongside other strategies like natural convection and conduction–radiation cooling [7]. The research continues to enhance heat pipe performance through innovations such as nanofluid integration and the use of phase change materials [1], reflecting the growing role of advanced functional materials for next-generation heat transfer systems.

Most heat pipes use a single material, such as copper, for its excellent thermal conductivity. However, in high-temperature or corrosive environments, copper alone lacks sufficient durability. A practical approach is to combine copper with SS316L – using Cu for the evaporator and condenser to maximize heat transfer, and SS316L for the adiabatic section where thermal conductivity is less critical. In this region, the superior corrosion resistance and mechanical strength of SS316L provide clear advantages.

Despite this functional complementarity, integrating Cu and SS316L remains challenging due to large differences in thermophysical and metallurgical properties, which can result in thermal mismatch, fusion imbalance, and intermetallic formation [8,9]. Recent studies on dissimilar TIG welding have emphasized that severe thermal mismatch and uneven heat distribution significantly affect HAZ stability and joint integrity. Pandey et al. reported that improper heat input during TIG of dissimilar metals promotes microstructural heterogeneity and premature failure, particularly in the weaker base metal side [10]. Recent studies have highlighted the critical role of heat input control in maintaining microstructural stability and joint reliability in TIG welding. Variations in current and welding speed were shown to significantly influence heat distribution and mechanical performance. Excessive heat input, particularly in copper-based alloys, can lead to microstructural degradation, emphasizing the need for precise parameter optimization [11–13].

Advances in solid-state welding and multi-metal additive manufacturing have shown promise in overcoming these issues [9,10]. yet, achieving reliable Cu–SS316L joints for heat pipes operating in the 300–600 °C range continues to demand further investigation, particularly regarding suitable joining techniques and material combinations that ensure both structural integrity and thermal efficiency [15].

The welding of Cu and SS316L is challenging due to large differences in thermal conductivity, thermal expansion, and metallurgical compatibility, which can cause fusion imbalance, brittle intermetallic formation, and uneven residual stresses. Recent studies emphasize that heat input in TIG welding plays a decisive role in joint quality. For example, investigations on TIG-welded SS304L have shown that heat input strongly influences temperature distribution, microstructural evolution, and tensile strength, with phase transformations and fracture modes confirmed through XRD and SEM analyses [16].

Previous studies on Cu and dissimilar materials, such as Cu-SS joints, have reported that increasing TIG welding heat input affects tensile strength, hardness, and thermal conductivity, with optimal strength observed at 1.2 kJ/mm due to improved penetration and metallurgical bonding [17]. The use of TIG welding with a nickel-based filler produced complex microstructures at the fusion zone, characterized by incomplete mixing and copper diffusion along stainless steel grain boundaries, resulting in tensile strength up to 143.7 MPa [18]. More recently, additive manufacturing with Selective Laser Melting has demonstrated defect-free Cu-SS316L joints with enhanced interface strength, attributed to Fe-rich nanoparticle formation and elemental diffusion supported by Marangoni convection [19].

Although various joining techniques, such as Electron Beam Welding, Magnetic Pulse Welding, Laser Beam Welding, Friction Stir Welding, TIG, and Shielded Metal Arc Welding, have been developed [20,21]. The TIG welding remains one of the most widely used and cost-effective methods for joining a wide range of metals and alloys. This process employs a non-consumable tungsten electrode and an inert shielding gas to protect the arc and molten pool from atmospheric contamination [22]. Also, TIG welding is particularly effective for stainless steels and non-ferrous alloys, offering high-quality welds [21]. A promising approach involves using a Cu-Si-based filler metal, which provides chemical compatibility with both Cu and SS substrates [23,24].

Dissimilar metal welding between Cu and SS316L remains technically demanding due to their contrasting thermal conductivities, coefficients of thermal expansion, and metallurgical compatibility [23,25]. These differences often result in fusion imbalance and brittle intermetallic phase formation. The TIG welding process is widely used for joining dissimilar metals, with welding parameters playing a critical role in determining joint quality. Among these parameters, heat input has been identified as a key factor influencing tensile strength, hardness, and bead width [26,27]. Optimal heat input settings can improve mechanical properties and microstructure [27–30]. The selection of filler material also significantly influences the resulting microstructure and mechanical properties of the weld joint [26,29].

Unlike previous studies that focused on homogeneous stainless-steel welds or evaluated individual properties separately, this work adopts a multidimensional approach that links welding heat input to both joint integrity and thermal performance. It provides a comprehensive assessment of how TIG welding with ERCuSi-A filler and controlled heat input affects the thermo-mechanical behavior of Cu/SS316L joints, including microstructural evolution, hardness, tensile strength, and thermal conductivity.

The effect of TIG welding parameters, particularly heat input, on the mechanical, microstructural, and thermal behavior of Cu/SS316L joints remains unclear, especially for heat pipe applications, where high thermal conductivity is crucial. The use of ERCuSi-A filler (a Cu–Si alloy) offers both chemical compatibility with Cu and SS316L and the potential formation of Cu–Si intermetallics that increase local hardness without sacrificing thermal conductivity.

The novelty of this work lies in quantifying how heat input affects thermal conductivity in the Cu/SS316L weld metal and in demonstrating its direct implications for heat pipe performance. Reduced conductivity in the welded joint region increases axial thermal resistance; therefore, the welded joint must be located outside the evaporator–adiabatic and adiabatic–condenser boundaries to avoid loss of efficiency. This study provides the first systematic correlation between heat input, weld microstructure, and thermal transport for Cu/SS joints intended for heat pipe systems.

MATERIALS AND METHODS

Materials

This study utilized Cu and SS 316L stainless steel as base materials, selected for their thermal compatibility and relevance to heat transfer applications, particularly in passive cooling heat pipe systems. ERCuSi-A filler wire was used due to its known physical and chemical compatibility for welding Cu to SS316L. The chemical composition of the materials used in this study is presented in Table 1. The chemical composition data were obtained using X-ray fluorescence (XRF) analysis in quantitative mode.

Cu and SS316L samples were cut to dimensions of 300 × 200 × 2.7 mm using a precision cutter. The joint surfaces were cleaned using fine sandpaper and an acetone solution to remove oxides, oil, and other contaminants. The welding was performed using a butt joint configuration. The root gap and bevel geometry are illustrated in Figure 1.

Figure 1 illustrates the joint geometry used for dissimilar Cu/SS316L welding. The copper side was prepared with a sharper bevel angle to facilitate sufficient heat concentration and ensure adequate fusion, considering copper's high thermal conductivity and rapid heat dissipation. In contrast, the SS316L side was machined with a less acute (non-sharp) bevel to avoid excessive penetration and dilution from the stainless steel, thereby maintaining weld pool stability and controlling elemental mixing. This asymmetric bevel design promotes balanced fusion behavior and improves joint integrity in Cu/SS316L dissimilar welding.

Table 1. Chemical composition

Name	Al (%)	Fe (%)	Si (%)	Cu (%)	Mn (%)	Co (%)	Ni (%)	Others
Cu	0.12	0.03	0.10	98.97	0.02	-	0.03	<0.2
Name	Mo (%)	Fe (%)	Cr (%)	Cu (%)	Mn (%)	Co (%)	Ni (%)	V (%)
SS 316L	2.078	69.15	16.82	0.08	1.21	0.37	10.23	0.070
Filler Rod: ERCuSi-A	-	-	3	-	-	-	-	97

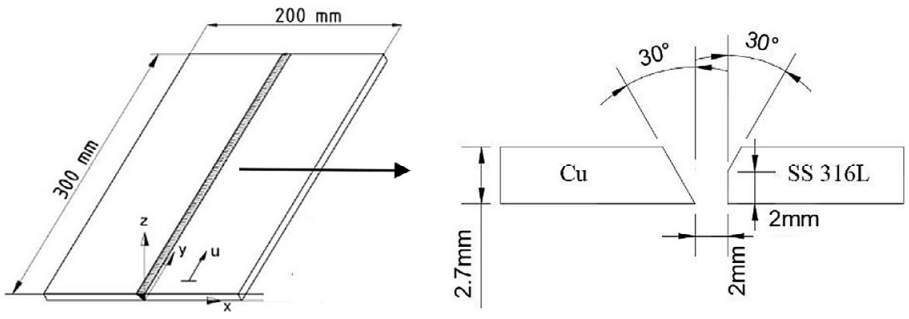

Figure 1. Joint geometry

TIG welding procedure

A butt joint between Cu and SS 316L was prepared with a V-groove bevel on both sides to ensure optimal weld penetration. Welding was performed using the TIG process in multiple passes, with varying heat inputs of 2.02, 2.04, and 1.41 kJ/mm. The selected heat inputs were derived from welding currents of 120–150 A, which are suitable for the 2.7 mm plate thickness. Preliminary welding trials outside this current range produced significant defects such as burn-through and excessive penetration. Thus, the selected currents and their corresponding heat inputs were chosen to ensure defect-free welding while enabling controlled variation in the thermal cycle.

The tungsten used is 2% Lanthanated tungsten, and the filler rod used is ERCuSi-A (2 mm). Ultra high purity (UHP) gas was supplied at a flow rate of 10 L/min to both the capping and root sides, as illustrated in Figure 2. The detailed welding parameters are summarized in Table 2.

The welding configuration used in this study is illustrated in Figure 2. The experiment employed a TIG system equipped with a dedicated TIG power source and a dual-argon shielding arrangement to ensure stable arc formation and oxidation-free weld surfaces during the joining of copper and SS316L. An argon supply was connected directly to the TIG torch to provide primary shielding over the molten weld pool, thereby protecting the arc region from atmospheric contamination and maintaining arc stability, which is particularly important due to the high thermal conductivity of copper.

In addition to the primary shielding, a secondary argon flow was introduced through a purging system positioned beneath the workpiece. This purging gas created an inert atmosphere on the root side of the joint, preventing oxidation and minimizing the formation of surface defects, especially on the SS316L side, which is highly susceptible to root oxidation at elevated temperatures. The workpieces, consisting of copper and SS316L plates arranged in a butt-joint configuration, were positioned on a fixture that provided adequate torch access and a consistent purging flow beneath the joint. This dual-shielding configuration ensured that both the upper weld region and the underside of the joint remained protected throughout the welding process. The combined effect of primary shielding and purging provided the controlled thermal and atmospheric conditions necessary for producing a clean and stable Cu/SS316L weld, thereby minimizing oxidation, contamination, and undesirable metallurgical reactions during joining. Welding parameters are shown in Table 2.

Table 2 shows that manual TIG welding was performed under identical conditions. Welding was conducted in two passes (root and capping) with a 2.0 mm ERCuSi-A filler rod to ensure adequate weld metal deposition for the 2.7 mm plate thickness while maintaining controlled heat input. UHP argon was used as the shielding gas at a flow rate of 10 L/min. The reported heat input values represent effective heat input derived from the applied welding parameters and were used for comparative analysis without introducing an explicit arc efficiency factor.

Before welding, the base materials were preheated to 100 °C to minimize thermal gradients and reduce the risk of cracking due to differential expansion [30]. Additionally, an interpass preheat temperature of 60 °C was applied before each welding layer to maintain thermal consistency and promote stable metallurgical bonding across the joint. Following the completion of welding, a non-destructive test (NDT) was performed using the penetrant testing method to detect surface defects such as cracks, open porosity, or lack of

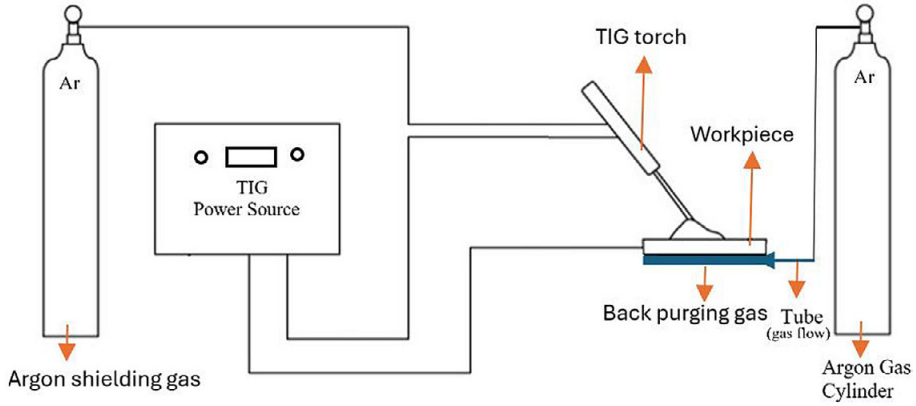

Figure 2. Material welding setup

Table 2. TIG welding parameters

Sample (No.)	Welding current (A)	Volt (V)	Welding speed (mm/min)	Welding heat Input (kJ/mm)
1#	150	12	76.69	1.41
2#	120	12	42.79	2.02
3#	135	12	47.61	2.04

fusion in the welded joint [31]. The procedure employed a solvent-removable penetrant system, in which excess dye was wiped off using a cloth moistened with a dedicated solvent before applying the developer, ensuring accurate and reliable inspection results.

Figure 3 shows the results of non-destructive testing conducted on the Cu/SS316L welded joints. Visual testing (VT) was performed first and revealed a uniform weld surface with no visible defects such as cracks, open porosity, or lack of fusion. This was followed by penetrant testing (PT) to detect possible small or micro surface-breaking defects. After the application of the developer, no indications appeared along the welded joint bead, confirming that no surface or micro defects were present in the welded joint.

Characterization of the welded joints

The Cu/SS316L dissimilar joints were evaluated through a comprehensive set of mechanical, thermal, and microstructural characterizations to investigate how different heat input levels influence joint performance. Metallographic preparation of cross-sectioned samples involved standard procedures, including grinding, polishing, and etching using a mixture of 5 g $FeCl_3$, 10 mL HCl, and 100 mL H_2O. Microstructural features were examined with a Carl Zeiss optical microscope and a FEI Quanta 250 scanning electron microscope (SEM), while elemental composition and diffusion across the interface were analyzed using energy dispersive x-ray spectroscopy (EDS).

Microhardness testing was performed using the Vickers method with a load of 1 kgf and a dwell time of 15 s to evaluate the hardness distribution across the TIG-welded Cu/SS316L joint. The selected load falls within the micro-Vickers range and is suitable for dissimilar joints, considering the higher hardness of SS316L compared with Cu, while providing sufficient indentation depth for reliable measurements in the welded joint metal and HAZ, where microstructures may be heterogeneous. Indentations were placed at 1 mm intervals along a transverse line from the SS316L base metal through the HAZ, weld metal, and into the Cu side, and the 2.7 mm plate thickness was sufficient to avoid substrate effects. Tensile test specimens were prepared in accordance with the ASTM E8/E8M standard, as illustrated in Figure 4. Tensile testing was performed using a Galda Bini™ Universal Testing Machine with a maximum load capacity of 100 kN. A total of nine specimens were tested, with three specimens evaluated for each heat input condition (1.41, 2.02, and 2.04 kJ/mm).

These combined characterization techniques provided insight into how thermal input from TIG welding impacts the welded joint integrity,

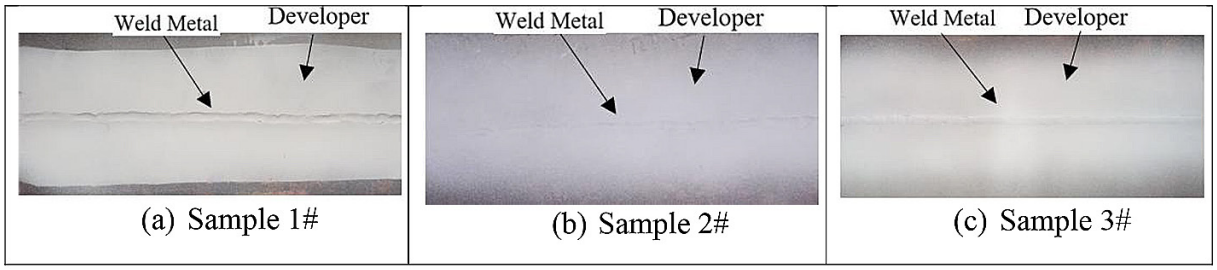

Figure 3. Penetrant test

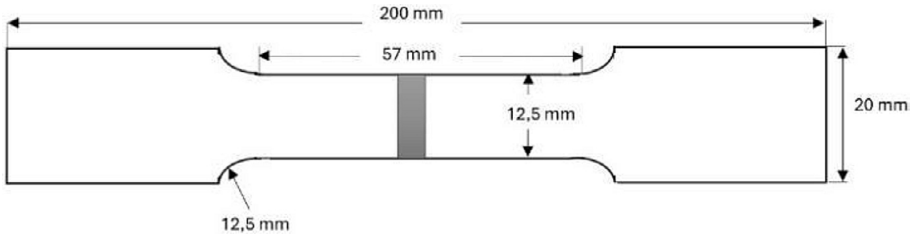

Figure 4. Tensile test specimen [32]

structure, and heat conduction capability, which are critical factors in heat pipe applications for passive nuclear cooling systems.

Thermal conductivity test

Thermal conductivity testing was conducted using the hot plate method, a technique for determining a material's ability to conduct heat. This method involves placing the test specimen between two metal plates with a controlled temperature difference. One plate is heated while the other is maintained at a lower temperature, as illustrated in Figure 5. Thermal conductivity is calculated based on the temperature difference between the plates and the heat flux through the specimen [33].

RESULTS AND DISCUSSION

Welding results

The welding of dissimilar materials of Cu - SS316L using the TIG process was successfully carried out with three different heat inputs: sample 1#, sample 2#, and sample 3#, as shown in Figure 6. Each heat input level produced distinct visual characteristics and weld bead geometries. Overall, the welded joint quality was considered satisfactory, with no visible surface defects such as undercut, open porosity, or incomplete fusion. The results of the penetrant test further confirmed the absence of welding defects.

Figure 6 shows the capping surface of the Cu/SS316L dissimilar welded joint, with Cu on the right and SS316L on the left. The weld bead is continuous and straight, with no visible surface defects such as undercut, porosity, or incomplete fusion. Oxidation discoloration on the Cu side reflects its higher thermal conductivity and different thermal response compared with SS316L.

Tensile strength

The tensile strength of the Cu–SS316L welded joints was analyzed by evaluating the effect of three different heat input levels. A total of nine tensile test specimens were tested, with three specimens evaluated at each heat input level (2.02, 2.04, and 1.41 kJ/mm). The tensile test results are presented in Figure 7.

Figure 7a. presents the tensile test results of the Cu/SS316L welded joints. Fracture consistently occurred on the copper side within or near the heat-affected zone (HAZ), as indicated by the dashed red box, while no fracture was observed in the weld metal, indicating that the weld metal was mechanically stronger than the copper base metal. This fracture behavior is attributed to the thermal cycle imposed by the selected welding current and heat input, where copper's high thermal conductivity promotes localized softening in the Cu HAZ. Error bars represent the standard deviation from three repeated tensile tests. This observation is consistent with the findings of Singh et al. [34] and Chethan et al. [35], who reported failure in

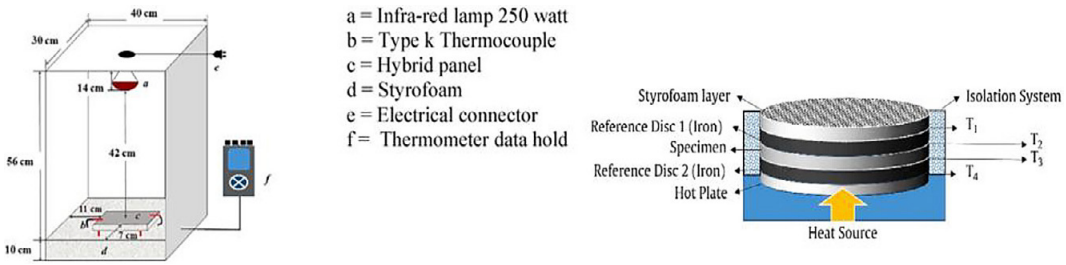

Figure 5. Thermal conductivity test schematic [33]

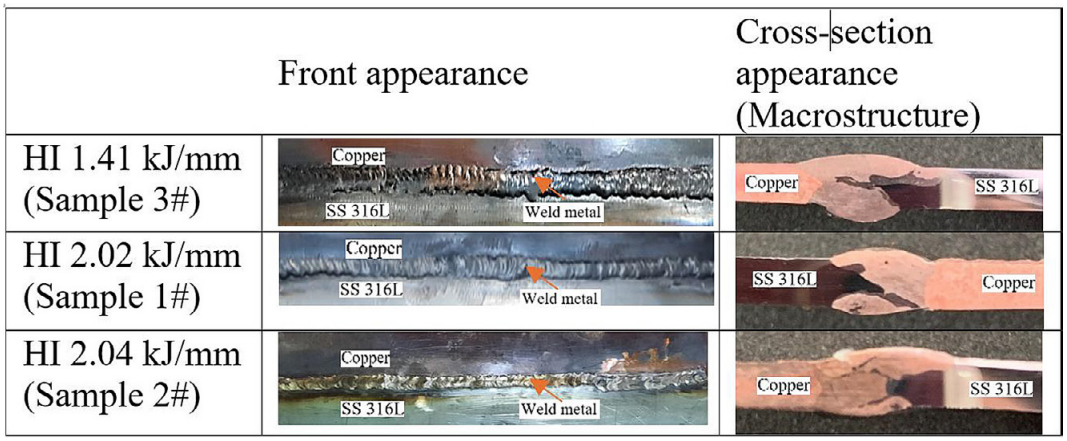

Figure 6. Macrostructural features of the Cu/SS316L welded join

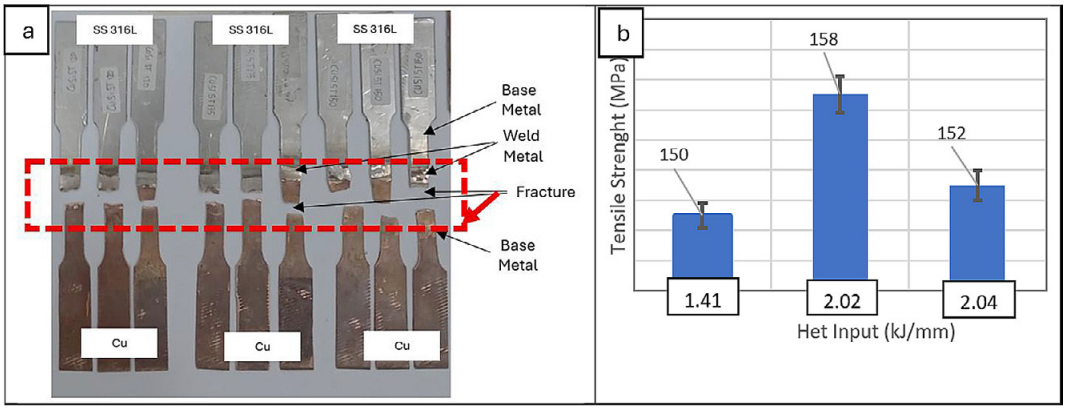

Figure 7. Tensile test results. (a) Fracture appearance, (b) Tensile strength vs heat input

the Cu HAZ due to thermal softening and grain coarsening under high local heat input. The absence of fracture within the welded joint metal confirms that the welded joint metal was mechanically stronger than the copper base material, highlighting the critical role of heat input control and confirming that the selected welding parameters produced an acceptable and mechanically sound Cu/SS316L welded joint [34,35]. As shown in Figure 7b, the ultimate tensile strength (UTS) exhibits a non-monotonic dependence on heat input, reaching a maximum value of 158 MPa at 2.02 kJ/mm, followed by lower strengths of 150 MPa at 1.41 kJ/mm and 152 MPa at 2.04 kJ/mm. These results indicate that the tensile response of the Cu/SS316L welded joints is sensitive to variations in heat input within the investigated range.

Overall, these results confirm that sample 1# offers optimal mechanical performance. The tensile strength results in this study align with the findings of Britto et al. [24], where failure consistently occurred in the HAZ region [24]. This

confirms the thermal sensitivity of SS in dissimilar joints with copper. Additionally, while ERCuSi-A was also used as the filler metal, both studies observed that increasing heat input does not linearly enhance joint strength, highlighting the importance of optimizing thermal input to prevent softening or grain coarsening in the HAZ.

Hardness analysis

This test aimed to observe hardness variation resulting from differences in cooling rates and thermal effects induced by variations in heat input as shown in Figure 8.

Figure 8 shows the microhardness distribution across the dissimilar Cu/SS316L TIG-welded joints using ERCuSi-A filler under different heat inputs. The Cu base metal exhibits the lowest hardness (~60–70 HV), consistent with its soft α-Cu matrix, while the SS316L base metal shows higher hardness (~100–110 HV) due to solid-solution strengthening. An increase in hardness is observed in the Cu HAZ, particularly at higher heat input, which is attributed to thermal exposure, element diffusion, and the formation of Cu–Si-rich precipitates. The weld metal region exhibits the highest hardness, with a peak value of ~165 HV at sample 1#, associated with rapid solidification and a fine dendritic structure, while samples 2# and 3# show a slight reduction due to grain coarsening and partial annealing. The SS316L HAZ displays moderate hardness enhancement (~130 HV), likely related to thermally induced strain hardening. These hardness trends are consistent with previous reports by Chang et al. [36] and Chethan et al. [35]. From a heat pipe perspective, sample 2# provides a favorable balance between mechanical integrity and thermal conduction, highlighting the importance of precise heat input control in Cu/SS316L dissimilar welding.

Microstructure observation

The welded joint microstructure critically influences the mechanical and functional performance of dissimilar joints, particularly for heat pipe applications. Optical microscopy was employed to examine the effects of heat input on microstructural evolution in Cu/SS316L TIG welds using ERCuSi-A filler, covering the weld metal, HAZ, and base metals. These observations clarify the relationship between welding parameters and the resulting hardness, tensile strength, and thermal conductivity, as shown for samples 1#, 2#, and 3# in Figure 9.

Figure 9a–c presents the microstructural evolution across the Cu/SS316L weldment observed under different heat inputs (1#, 2#, and 3#). Under the lowest heat input condition (Figure 9a), the Cu HAZ exhibits relatively fine grains with a clearly defined fusion boundary, indicating limited thermal exposure. The weld metal is dominated by a Cu-rich matrix with generally fine and uniformly distributed SS-rich particles; although a few relatively coarse SS particles are observed, their limited number and isolated distribution prevent the formation of continuous networks or significant porosity, reflecting stable solidification and a minimal influence on the overall mechanical and thermal properties. The SS316L HAZ shows only minor microstructural changes with limited grain growth, indicating that the applied heat input remains within a controlled range. Overall, this condition results in the most homogeneous microstructure.

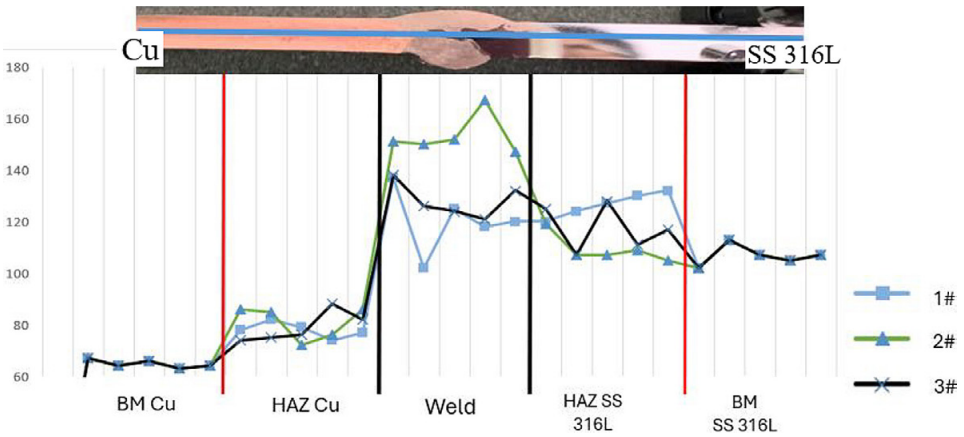

Figure 8. Microhardness (HV) distribution across Cu/SS316L welded joints

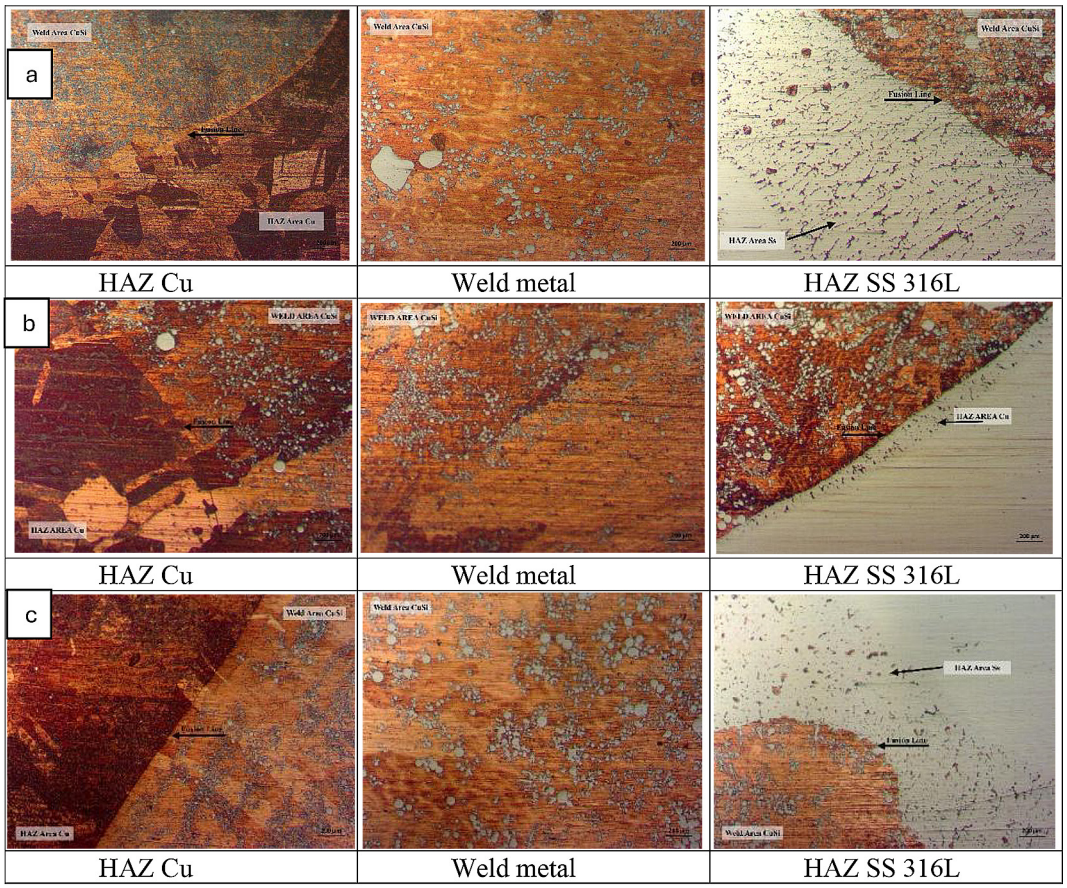

Figure 9. Microstructure. (a) 1#, (b) 2#, (c) 3#

With increasing heat input (Figure 9b), the Cu HAZ exhibits more pronounced grain coarsening compared with condition (9a), indicating increased thermal exposure. The weld metal shows a higher number and larger SS-rich particles with a progressively non-uniform distribution, along with indications of microporosity, suggesting a reduced cooling rate. In the SS316L HAZ, increased grain boundary activity is observed, although without severe degradation. This microstructural condition reflects a trade-off between improved fusion and the onset of microstructural heterogeneity. Under the highest heat input condition (Figure 9c), the Cu HAZ exhibits the most pronounced grain coarsening, reflecting excessive thermal exposure. The weld metal shows coarser and increasingly agglomerated SS-rich particles accompanied by higher microporosity, indicating non-uniform solidification and intensified elemental diffusion. The SS316L HAZ undergoes more evident grain growth, suggesting an increased risk of mechanical and thermal property degradation. Overall, this microstructure indicates that the applied heat input exceeds the optimal condition.

These microstructural observations are consistent with the review by Amirhossein et al. [37], which highlights the complexity of achieving metallurgically sound dissimilar joints between copper and stainless steel. Their findings emphasize that controlling fusion line morphology, elemental interdiffusion, and intermetallic formation is critical to ensuring joint integrity, especially when welding highly conductive materials like copper.

To further investigate the microstructural features and elemental distribution, SEM–EDS characterization was performed on the specimen welded at samples 1#, 2#, and 3#, are presented in Figure 10.

Figure 10a shows a clearly defined fusion boundary between the welded joint metal and the SS316L base metal at 500× magnification. The welded joint metal exhibits a more homogeneous morphology dominated by fine granular solidification structures from the Cu-based ERCuSi-A filler, while the SS316L side displays a coarser austenitic structure. The microstructural transition near the fusion line appears sharp, with no evidence of a thick intermetallic layer, although a

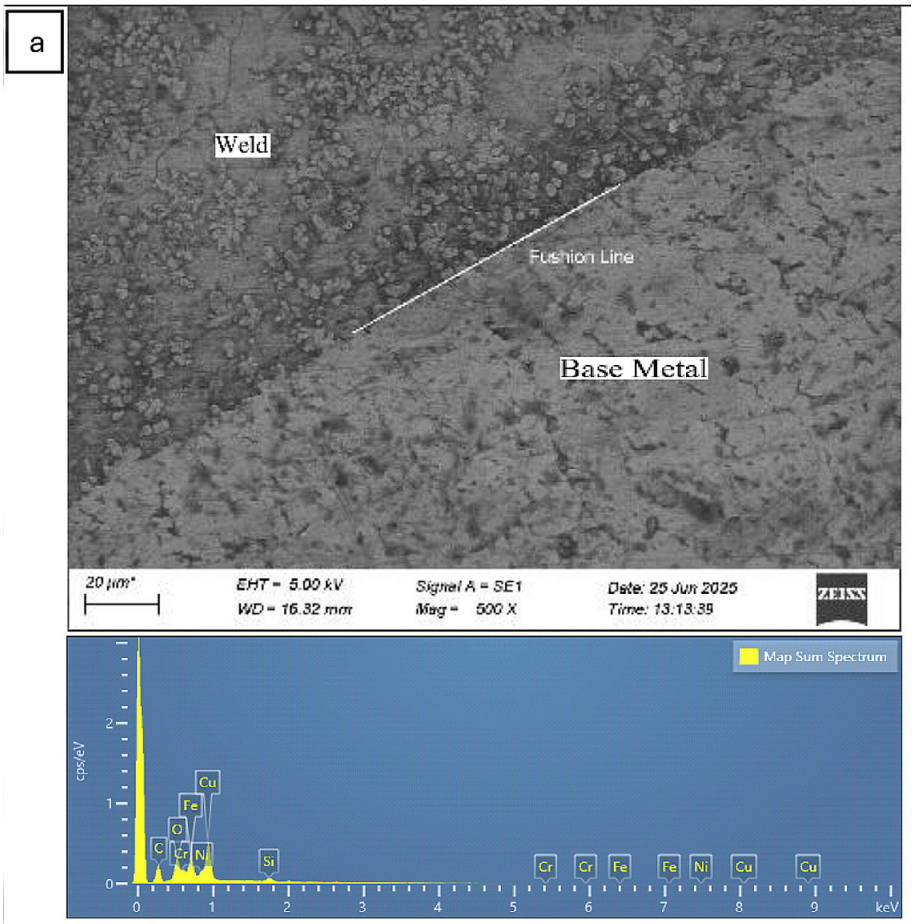
a
Weld
Fushion Line
Base Metal
20 µm*
EHT = 5.00 kV
WD = 16.32 mm
Signal A = SE1
Mag = 500 X
Date: 25 Jun 2025
Time: 13:13:39
ZEISS
Map Sum Spectrum
cps/eV
Cu
Fe
O
C
Cr
Ni
Si
Cr
Cr
Fe
Fe
Ni
Cu
Cu
keV

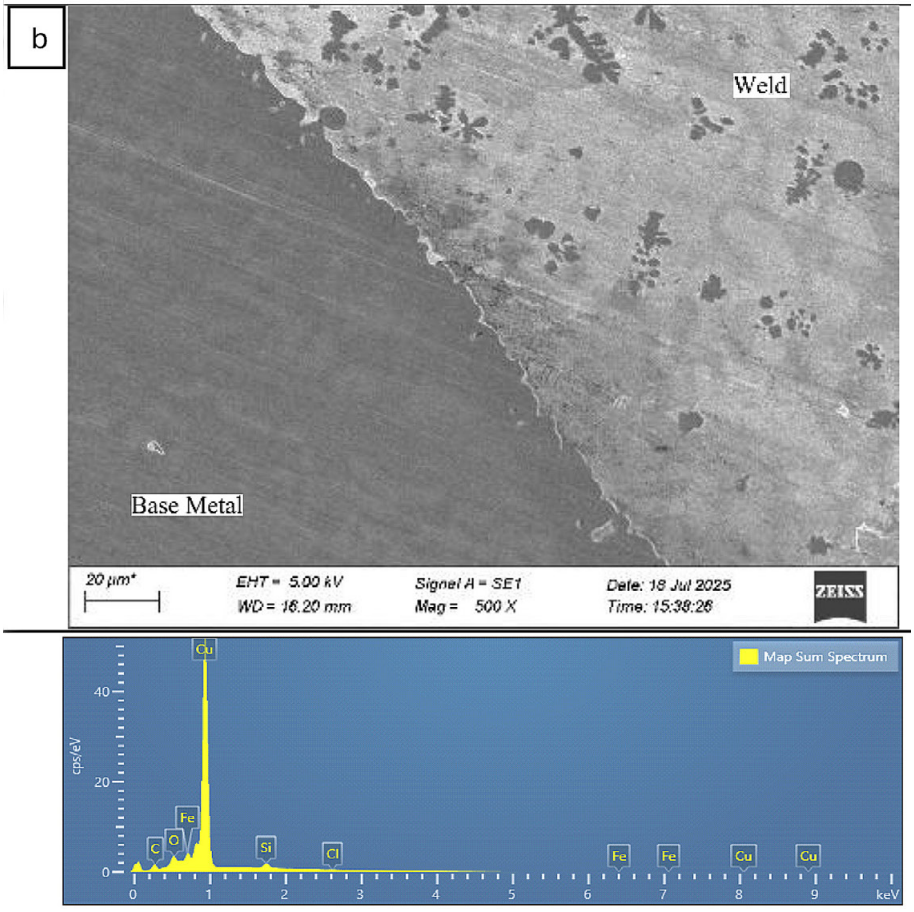
b
Weld
Base Metal
20 µm*
EHT = 5.00 kV
WD = 16.20 mm
Signal A = SE1
Mag = 500 X
Date: 18 Jul 2025
Time: 15:38:26
ZEISS
Map Sum Spectrum
cps/eV
Cu
Fe
C
O
Si
Cl
Fe
Fe
Cu
Cu
keV

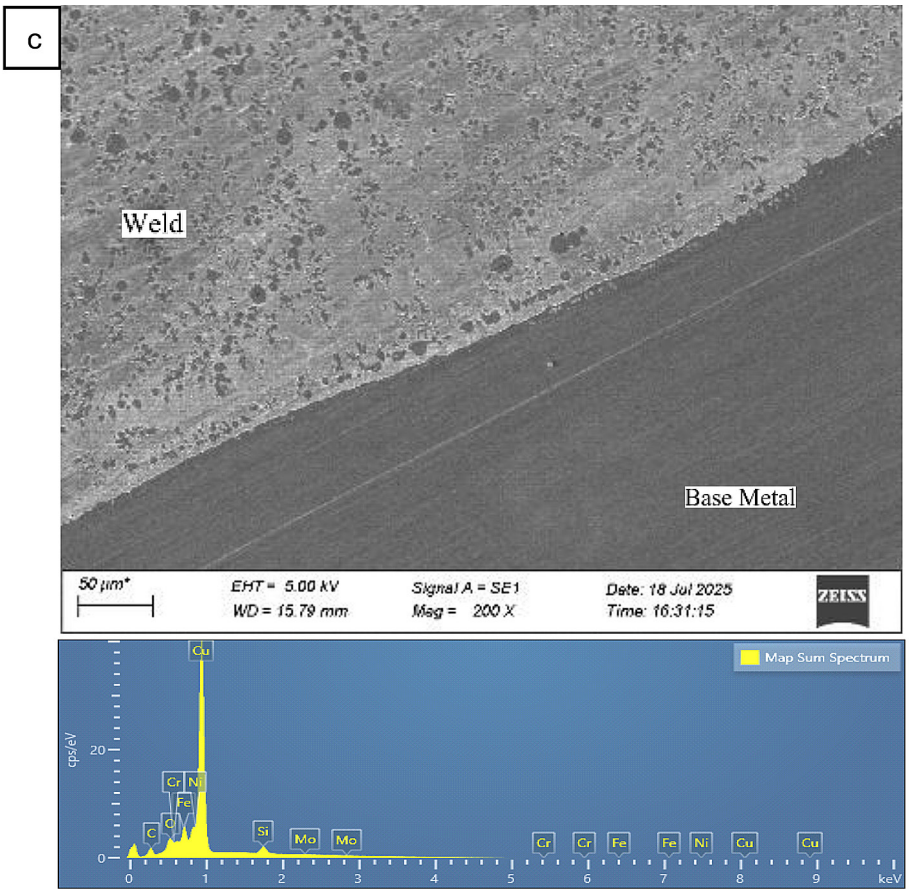

Figure 10. SEM-EDS on welded joints at: Sample (a) 1# (b) 2# (c) 3#

thin transition zone is present due to limited elemental diffusion during welding. The EDS Map Sum Spectrum identifies Cu as the dominant element in the welded joint metal, originating from both the Cu base metal and the ERCuSi-A filler, along with Fe, Cr, and Ni from the SS316L base metal. The presence of Si confirms the contribution of the filler, whereas O indicates localized oxidation. The low-intensity Cr and Ni peaks suggest minimal diffusion at the applied heat input of 2.02 kJ/mm, and no characteristic peaks of newly formed intermetallic compounds are detected. Overall, these results confirm that Cu–SS316L welding at 2.02 kJ/mm produces a clean fusion boundary, limited elemental interdiffusion, and a uniform Cu-based weld metal solidification.

Figure 10b shows the 500× microstructure of the Cu/SS316L joint welded at 2.04 kJ/mm. The fusion boundary is still clear, but the welded joint metal exhibits a more heterogeneous morphology with coarser solidification features and Cu-rich regions, reflecting increased thermal exposure and slower cooling. The SS316L base metal maintains its austenitic structure, while the transition zone becomes slightly wider, indicating greater elemental mixing than at lower heat input. Localized island-type segregations appear near the fusion line, though no continuous intermetallic layer is present. EDS mapping confirms Cu as the dominant weld-metal element, with Fe, Cr, and Ni peaks showing more pronounced diffusion from SS316L compared with lower heat inputs. Si originates from the ERCuSi-A filler, and minor oxygen peaks suggest light oxidation. Importantly, no distinct intermetallic peaks are detected. Overall, welding at 2.04 kJ/mm produces a wider transition zone, increased diffusion, and a more heterogeneous weld metal, yet the fusion boundary remains intact and free of detrimental intermetallic layers, indicating acceptable metallurgical compatibility at this heat input.

Figure 10c shows the microstructure of the Cu/SS316L joint welded at 1.41 kJ/mm (200×). The fusion boundary is smooth and well-defined, with minimal distortion. The welded joint metal displays a fine, uniform granular structure, indicating faster cooling at low heat input. The SS316L base metal retains its austenitic morphology with a very narrow transition zone, reflecting

limited thermal penetration and elemental mixing. EDS mapping confirms that Cu dominates the welded joint metal, originating from both the Cu base and the ERCuSi-A filler. Fe, Cr, Ni, and Mo from SS316L appear only in low intensities, showing minimal diffusion, while Si corresponds to the Cu–Si filler. No peaks indicating intermetallic formation are detected. Overall, SEM–EDS results show that 1.41 kJ/mm produces a clean interface, minimal interdiffusion, and a refined weld structure – indicating that low heat input effectively suppresses dilution and prevents brittle intermetallic formation in Cu/SS316L joints.

Thermal conductivity

Thermal conductivity is crucial for heat pipe performance, especially in high-temperature passive cooling systems. In Cu/SS316L joints, it is strongly affected by the welding thermal cycle and the resulting microstructure. Three specimens – each representing a different heat input – were tested, with three measurements per specimen. Thermal conductivity for samples 1#, 2#, and 3# was obtained using the hot plate method, as shown in Figure 11.

Figure 11 shows a marked contrast in thermal conductivity between the base materials, with copper exhibiting the highest value (~398–400 W/m·K), consistent with its high electron mobility, while SS316L shows a significantly lower value (~16 W/m·K), which inherently challenges thermal uniformity in the welded joint zone. After welding, a general reduction in thermal conductivity was observed in all joints, which is attributed to structural heterogeneity and the formation of Cu–Si intermetallic precipitates. The thermal conductivity values of the welded joints are presented as mean ± standard deviation (n = 9), and the relatively small and comparable standard deviation across different heat input conditions indicates good repeatability and measurement stability. As shown in Figure 11, the lowest thermal conductivity was recorded for sample 3# (2.04 kJ/mm). This reduction is associated with microstructural (Figure 9) inhomogeneity in the weld metal, where Cu–Si precipitates act as electron-scattering sites that impede heat transfer. Similar observations were reported by Sun and Dilger [38], who demonstrated that microstructural heterogeneity significantly degrades thermal conductivity in welded joints, leading to higher thermal gradients and non-uniform cooling. Armentani et al. [39] further noted that reduced thermal conductivity promotes localized heat retention and increases residual stress.

In contrast, sample 1# exhibited the highest thermal conductivity among the welded joints, while sample 2# showed an intermediate value, indicating that thermal transport is highly sensitive to heat input and microstructural evolution. These results are consistent with Ley et al. [40], who emphasized that welding parameters strongly influence the thermal behavior of dissimilar joints. The present findings highlight that, beyond mechanical strength, thermal conductivity must be carefully considered for heat pipe applications, as reduced conductivity, particularly in sample 3#, may increase axial thermal resistance during steady-state operation.

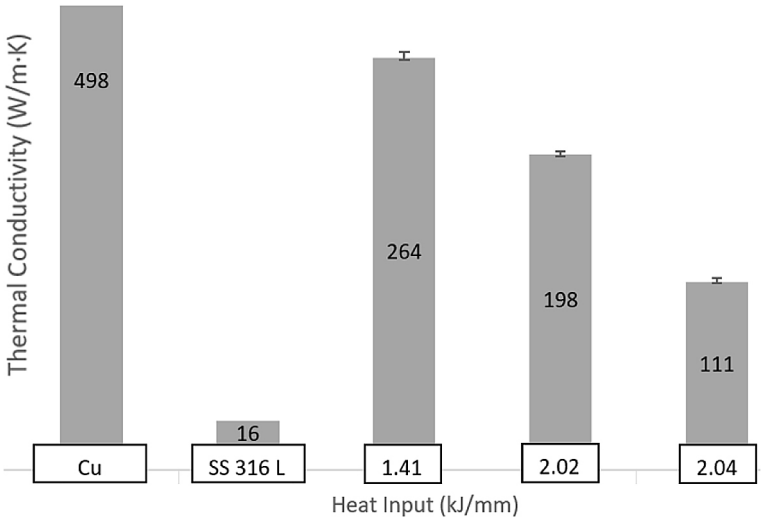

Figure 11. Thermal conductivity

CONCLUSION

This study examined the effect of TIG welding heat input on the microstructure, mechanical properties, and thermal conductivity of dissimilar Cu/SS316L welded joints using an ERCuSi-A filler for heat pipe applications. The results confirm that heat input critically governs microstructural uniformity, elemental diffusion, and joint performance. Tensile testing showed that fractures consistently occurred in the Cu heat-affected zone rather than in the weld metal, indicating that the weld metal was mechanically stronger than the copper base material. Among the investigated conditions, the lowest heat input (1.41 kJ/mm) provided the most favorable balance, resulting in stable mechanical behavior and the highest thermal conductivity of the welded joints. In contrast, excessive heat input promoted microstructural heterogeneity and Cu–Si precipitate formation, which disrupted heat conduction and reduced thermal performance. These findings demonstrate that thermal conductivity, in addition to mechanical strength, must be carefully considered when welding Cu/SS316L joints for heat pipe systems. Future work will focus on thermal cycling and long-term reliability under representative service conditions.

Acknowledgments

The first author sincerely acknowledges the support provided by the National Research and Innovation Agency (BRIN) through the "Degree by Research Program" under contract number 27/II/HK/2024. Furthermore, the authors extend their deepest appreciation to Diponegoro University and the PRTRN BRIN management team for their invaluable contributions toward the successful completion of this research. In addition, the authors would like to thank the financial support provided by Kementerian Pendidikan Tinggi, Sains, dan Teknologi Republik Indonesia under the Regular Fundamental Research Scheme, through grant numbers 037/C3/DT.05.00/PL/2025 and 508/C3/DT.05.00/PL-PNL/2025.

REFERENCES

1. Jose J, Hotta TK. A comprehensive review of heat pipe: Its types, incorporation techniques, methods of analysis and applications. Therm Sci Eng Prog. 2023;42:101860. https://doi.org/10.1016/j.tsep.2023.101860
2. Apriandi N, Rozi K, Kusuma MH, Kiono BFT, Raharjanti R, Pambudi YDS, et al. A PAGER framework-enhanced bibliometric analysis of global nuclear desalination research trends (2005–2024). Desalination. 2025;118564. https://doi.org/10.1016/j.desal.2025.118564
3. Maghrabie HM, Olabi AG, Alami AH, Al Radi M, Zwayyed F, Wilberforce T, et al. Numerical simulation of heat pipes in different applications. Int J Thermofluids. 2022;16:100199. https://doi.org/10.1016/j.ijft.2022.100199
4. Kusuma MH, Haryanto D, Hatmoko S, Pambudi YDS, ButarButar SL, Putra N, et al. Experimental investigation of thermal characteristics on a new loop pipe model for passive cooling system. Therm Sci Eng Prog. 2024;50:102555. https://iopscience.iop.org/article/10.1088/1742-6596/1198/2/022055
5. Wahlquist S, Hansel J, Sabharwall P, Ali A. A critical review of heat pipe experiments in nuclear energy applications. Nucl Sci Eng. 2023;197(5):719–52.
6. Kusuma MH, Putra N, Antariksawan AR, Koestoer RA, Widodo S, Ismarwanti S, et al. Passive cooling system in a nuclear spent fuel pool using a vertical straight wickless-heat pipe. Int J Therm Sci. 2018;126:162–71.
7. Guillen DP. Review of passive heat removal strategies for nuclear microreactor systems. Nucl Technol. 2023;209(sup1):S21–40.
8. Joshi GR, Badheka VJ, Pathak V, Mohan DG. A comprehensive review of fusion welding for joining copper with stainless steel. J Adhes Sci Technol. 2025;39(5):635–86.
9. Joshi GR, Badheka VJ, Darji RS, Oza AD, Pathak VJ, Burduhos-Nergis DD, et al. The joining of copper to stainless steel by solid-state welding processes: a review. Materials (Basel). 2022;15(20):7234.
10. Kumar A, Singhal A, Sirohi S, Fydrych D, Pandey C. Pulsed current GTAW Inconel 625/AISI 304 L steel dissimilar joint: Microstructure and mechanical properties. J Constr Steel Res. 2025;231:109602.
11. Gopi S, Mohan DG, Natarajan E. Mechanical and corrosion properties of friction stir welded and tungsten inert gas welded phosphor bronze. Adv Mater Sci. 2023.
12. Toaldo PH, Ferreira ASF, Verastégui RN, Pukasiewicz AGM. Evaluation of the processing parameters influence on the additive manufacturing of VP50IM steel by PCGTAW. Soldag Inspeção. 2024;29:e2901.
13. Szewczyk A, Jarska R, Rogalski G. Effect of heat input on distortion and morphology of tungsten inert gas welded joints in AISI 304L stainless steel. Adv Sci Technol Res J. 2025;19(9):92–104.
14. Lee K, Doddapaneni VVK, Mirzababaei S, Pasebani S, Chang CH, Paul BK. Multi-metal additive manufacturing of selectively doped 316 L stainless steel-copper composite using hybrid laser powder bed fusion. Addit Manuf. 2024;86:104202.

15. Werner TC, Yan Y, Karayiannis T, Pickert V, Wrobel R, Law R. Medium temperature heat pipes–Applications, challenges and future direction. Appl Therm Eng. 2024;236:121371.
16. Kumar P, Sinha AN, Hirwani CK, Murugan M, Saravanan A, Singh AK. Effect of welding current in TIG welding 304L steel on temperature distribution, microstructure and mechanical properties. J Brazilian Soc Mech Sci Eng. 2021;43(7):369.
17. Azwinur A, Kusuma MH, Usman U, Dharma S. Effects of heat input on mechanical properties, microstructures and thermal conductivity of copper alloy in gas tungsten arc welding technology. Adv Sci Technol Res J [Internet]. 2025;16(6). Available from: https://www.astrj.com/Effects-of-Heat-Input-on-Mechanical-Properties-Microstructures-and-Thermal-Conductivity,203367,0,1.html
18. Thomas N, Mathew A, George K, Thomas N, Thampi S, Biradar A, et al. Microstructural and mechanical properties evaluation of tungsten inert gas-welded 316 stainless steel and pure copper joint. Metallogr Microstruct Anal. 2020;9:678–84.
19. Telasang G, Narayanaswamy S, Bathe R. Selective laser melting of stainless steel on the copper alloy: an investigation of the interfacial microstructure and mechanical properties. J Manuf Process. 2022;80:920–9.
20. Weman K. Welding processes handbook. Elsevier; 2011.
21. Periyasamy PS, Sivalingam P, Vellingiri VP, Maruthachalam S, Balakrishnapillai V. A review of traditional and modern welding techniques for copper. Weld Int. 2024;38(10):673–85.
22. Tseng KH, Hsu CY. Performance of activated TIG process in austenitic stainless steel welds. J Mater Process Technol. 2011;211(3):503–12.
23. Joseph GB, Valarmathi TN, Martin M, Marthandan N. Study the mechanical properties of stainless steel & copper joint by tungsten inert gas welding. Mater Today Proc. 2021;44:3738–43.
24. Cheng Z, Liu H, Huang J, Ye Z, Yang J, Chen S. MIG-TIG double-sided arc welding of copper-stainless steel using different filler metals. J Manuf Process. 2020;55:208–19.
25. Cheng Z, Huang J, Ye Z, Chen Y, Yang J, Chen S. Microstructures and mechanical properties of copper-stainless steel butt-welded joints by MIG-TIG double-sided arc welding. J Mater Process Technol. 2019;265:87–98.
26. Assefa AT, Ahmed GMS, Alamri S, Edacherian A, Jiru MG, Pandey V, et al. Experimental investigation and parametric optimization of the tungsten inert gas welding process parameters of dissimilar metals. Materials (Basel). 2022;15(13):4426.
27. Ghumman KZ, Ali S, Din EU, Mubashar A, Khan NB, Ahmed SW. Experimental investigation of effect of welding parameters on surface roughness, micro-hardness and tensile strength of AISI 316L stainless steel welded joints using 308L filler material by TIG welding. J Mater Res Technol. 2022;21:220–36.
28. Yelamasetti B, Devi BTL, Saxena KK, Sonia P, Vardhan TV, Sree NS, et al. Mechanical characterization and microstructural evolution of Inconel 718 and SS316L TIG weldments at high temperatures. J Mater Res Technol. 2024;32:196–207.
29. Li J, Zhou P, Shi H, Wang L. Influence of filler metal on microstructure and properties of titanium/copper weld joint by GTAW weldments. Mater Sci Eng A. 2022;833:142508.
30. Gavrish PA, Perig A V. Improvement of the heat state in welding copper with steel. Adv Mater Process Technol. 2020;6(4):703–17.
31. Roshan CC, Raghul C, Ram HV, Suraj K, Solomon J. Non-destructive testing by liquid penetrant testing and ultrasonic testing – A review. Int J Adv Res Ideas Innov Technol. 2019;5:694–7.
32. ASTM. E8/E8M. Standart Test Methods for Tension Testing of Metallic Material. West Conshohocken, United States: American Society for Testing Methods; 2009.
33. Jofrishal J, Adlim M, Yusibani E, Akhyar A, Rahmayani RFI, Fajri R. Preparation and characterization of indoor heat blockage panel composites made of polyurethane-hybrid-foam-concrete and rice-husk-ash. Heliyon. 2023;9(8).
34. Singh G, Saxena RK, Pandey S. An examination of mechanical properties of dissimilar AISI 304 stainless steel and copper weldment obtained using GTAW. Mater Today Proc. 2020;26:2783–9.
35. Roy C, Pavanan V V, Vishnu G, Hari PR, Arivarasu M, Manikandan M, et al. Characterization of metallurgical and mechanical properties of commercially pure copper and AISI 304 dissimilar weldments. Procedia Mater Sci. 2014;5:2503–12.
36. Sadeghian A, Iqbal N. A review on dissimilar laser welding of steel-copper, steel-aluminum, aluminum-copper, and steel-nickel for electric vehicle battery manufacturing. Opt Laser Technol. 2022;146:107595.
37. Sun J, Dilger K. Influence of thermal conductivity on the predicted temperature fields in welding of steels. Int J Therm Sci. 2024;202:109066.
38. Armentani E, Esposito R, Sepe R. The effect of thermal properties and weld efficiency on residual stresses in welding. J Achiev Mater Manuf Eng. 2007;20(1–2):319–22.
39. Ley FH, Campbell SW, Galloway AM, McPherson NA. Effect of shielding gas parameters on weld metal thermal properties in gas metal arc welding. Int J Adv Manuf Technol. 2015;80:1213–21.